Quantum interference structures in trapped-ion dynamics beyond the Lamb-Dicke and rotating wave approximations

Dong Wang,[1] Tony Hansson,[1] Åsa Larson,[1] Hans O. Karlsson,[2] and Jonas Larson[3]

[1]*Department of Physics, AlbaNova University Center, Stockholm University, SE-106 91 Stockholm, Sweden*

[2]*Department of Physical and Analytical Chemistry, Quantum Chemistry, Uppsala University, Box 518, SE-751 20 Uppsala, Sweden*

[3]*ICFO-Institut de Ciències Fotòniques, E-08860 Castelldefels, Barcelona, Spain*

We apply wave-packet methods to study an ion-trap system imposing neither the rotating wave nor the Lamb-Dicke approximations. By this approach we show the existence of states with restricted phase-space evolution as a genuine consequence of quantum interference between wave-packet fractions. A particular instance of such a state oscillates between maximal entanglement and pure disentanglement between the constitute subsystems, where the characteristic crossover time is very rapid. Over longer time periods the dynamics of these states exhibits collapse-revival patterns with well-resolved fractional revivals in autocorrelation, inversion, and entanglement.

I. INTRODUCTION

Progress in research fields, such as laser cooling, production, and controlling subfemtosecond laser pulses, manufacturing of solid-state devices, and so forth, render possible experiments of novel quantum characters. A key model in quantum optics is the harmonically trapped ion pumped by external lasers [1], which successfully has been used to study pure quantum phenomena in experiments [2–5]. Both the internal electronic structure of the ion and its center-of-mass motion are treated quantum mechanically, and it is possible to tune experimental parameters such that a single or few electronic transitions in the ion can be isolated and coherently coupled to the motion. The spatial profile of the driving laser, either a standing wave (SW) or a traveling wave (TW), effectively reshapes the trapping potentials. In particular, a unitary transformation of the regular one-dimensional ion Hamiltonian with TW pumping may result in two equally shifted and equally displaced coupled harmonic oscillators [6,7], whereas SW fields in general generate coupled potentials with a more complex shape. In addition, a fairly new proposal, verified by experiments, is to place the trap inside a high-Q microcavity such that it is the cavity field driving the trapped ion [8,9]. Even Bose-Einstein condensates have been successfully trapped and coherently coupled to a single-cavity mode [10].

In most theoretical work pertaining to both the SW and TW cases, approximations are imposed in order to obtain analytical or semianalytical results valid in different parameter regimes.

(i) *The Lamb-Dicke* (LD) *regime*. In this regime the wavelength of the classical laser field is long compared to the extent of the confining harmonic trap and an expansion in the small *Lamb-Dicke parameter* η of the mode profile function is made [11–16].

(ii) *The rotating wave approximation* (RWA) *regime*. Here, a basis is defined in which the involved time scales differ considerably and, once in the interaction picture, fast oscillating terms are neglected [17–21]. This assumes that the particular system can be separated into a "slow" and a "fast" part, which puts constraints on the constituent frequencies: the trap frequency ω, ion transition frequency Ω, laser frequency ω_L, and Rabi frequency λ (laser-ion coupling amplitude).

(iii) *Strong- and weak-excitation regimes*. These are the limiting situations of either a very large or small dimensionless parameter λ/ω [22–24] corresponding to, respectively, strong or weak pumping of the ion. It should be noted that this definition assumes a moderate number of phonon excitations ($n \lesssim 10$); otherwise, the effective Rabi frequency may become relatively large even in the weak-excitation regime. This, in fact, is the case of the current work.

Typically, the parameter regimes for which the above approximations are justified overlap and, in particular, there are regions in which none of them are valid. In many studies, one of the approximations is applied and one considers dynamics "beyond" the others. This, however, can be misleading since one is often in a parameter regime where also the nonimposed approximations could in principle have been implemented. Recently, Liu *et al.* [25] showed that the ground state of a TW pumped trapped ion may be considerably lowered when both the RWA and LD approximation are invalid. In the current work we use a fully numerical method and therefore no approximations are imposed. We discuss, nevertheless, the various parameter regimes as well as introduce an additional approximation—namely, the *adiabatic approximation*—to provide further insight into the quantum dynamics. It is commonly thought that the dynamics, in contrast to the simple cases of the validity regimes discussed above, becomes irregular beyond these approximations. We will here show that this is indeed not always true.

Theoretical and experimental research on trapped ions has been concerned with both SW and TW driving, with the main focus on the latter. Examples include state preparation of nonclassical vibrational states such as quantum superposition (so-called "Schrödinger cat") states or Fock states for both TW [11,19,21,23,24] and SW [12,13,20,26] pumping, collapse-revivals in the TW [3,15] and SW [14] cases, state measurement [16], and quantum information processing [4,27].
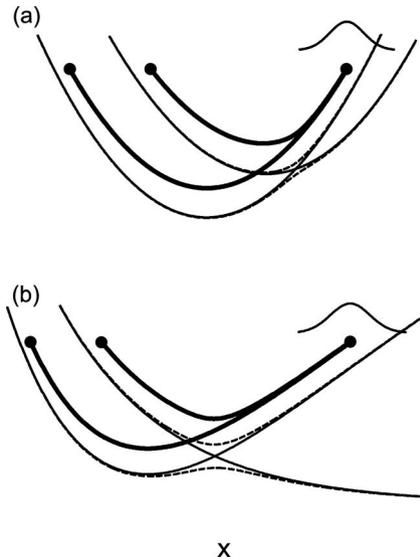
FIG. 1. Schematic illustration of bistable wave-packet motion: the wave packet starts out in one diabatic state, splits at the crossing point, and returns to the crossing where the parts interfere to reproduce the initial wave packet after one classical period of an individual potential well. The upper plot (a) displays the example of two bound states, typical of our trapped-ion system, while the lower one (b) shows a bound state coupled to a repulsive one, which is a system of relevance to molecular dynamics [like (a)], where *x* represents the internuclear distance.

The above-mentioned theoretical works almost exclusively employed the formalism of vibrational creation and annihilation operators for the harmonic trap. We, on the other hand, will reformulate the model in terms of ionic center-of-mass position and momentum, casting the problem into one of two coupled harmonic oscillators. In particular, we will study the coupled dynamics of an ion wave packet evolving on the two potentials in the case of SW pumping. For a one-dimensional system, such as the one we consider, it resembles an idealized diatomic molecule for which only two coupled bound electronic states are taken into account. A similar analogy, but between a diatomic molecule and a cavity QED model, was pointed out in [28,29], works that also made use of the wave-packet method. As the standard viewpoints and methods applied in quantum optics and molecular physics are rather different, we discuss them and their relation in some depth with the aim to facilitate branching out and combining the two research fields.

Since the pioneering work in the 1970s by Heller [30], wave-packet techniques have been used especially in molecular and chemical physics research [31]. It is not always possible to separate the dynamics in isolated electronic states, and the evolution on coupled electronic potentials has to be considered; couplings could be of, e.g., vibronic, spin-orbit, or rotational nature or induced by an external laser field. In Fig. 1, we display two schematic examples of coupled, bound-bound potentials in (a) and bound-repulsive potentials in (b). The solid potential curves are diabatic, while the corresponding adiabatic ones are shown as dashed curves (for a proper definition, see Sec. II B). When the wave packet propagates on the coupled potentials, inter-

ference effects will occur. In the bound-repulsive system, one such effect manifests itself as unexpectedly long-lived vibrational states [32]. This takes place when the interference restricts the wave-packet evolution in such a way that the repulsive part of the system at the right side of the curve crossing is not reached, indicated with the heavy solid lines in Fig. 1(b). We call this a *bistable* motion [33–36]. Similar interference effects can also occur in a system consisting of two coupled bound states, in which case the wave packet always returns to the same diabatic potential after one oscillation [see Fig. 1(a)]. In *astable* motion (not shown), the wave packet starts in one diabatic state, splits at the curve crossing, and when it returns to the curve crossing it recombines in such a way that it switches completely to the other diabatic state. Consequently, astable motion cannot exist in a system comprising coupled bound-repulsive states. We have previously carried out a numerical wave-packet study of the dynamics of bistable trajectories [36] and found that the trajectories can be exceedingly long lived with sharp fractional and full revivals.

Here we extend our former work and explore the dynamics of a system describing a trapped ion driven by a standing wave. We point out that also in such a system bistable motion exists and investigate the short- and long-term evolution of the system under this interference condition.

The outline of the article is as follows. We begin Sec. II by presenting the trapped-ion model Hamiltonian, as it is generally stated in quantum optics, and discuss parameter regimes and the corresponding approximations—rotating wave, Lamb-Dicke, weak and strong excitation, and adiabatic. It is shown how the Hamiltonian relaxes to an effective one mimicking the acclaimed Jaynes-Cummings (JC) model of quantum optics [37]. The relation between frequently used bases are considered in Sec. II B for which we define the corresponding potential curves. This enables us to obtain a deeper intuition about the dynamics and physical properties of the coupled system. The analogous molecular electronic states with their potential energy curves and couplings are also discussed, briefly. The following section, Sec. III, is dedicated to our numerical results. First we define the concept of bistable motion and then show how it enters into the trapped-ion model. For short time scales, we show in Sec. III A that this type of dynamics oscillates between an entangled (can be made maximally entangled) and a disentangled state. We analyze the nature of the wave-packet evolution around the potential curve crossing in terms of the ionic inversion, the autocorrelation, and the von Neumann entropy. For very long times (Sec. III B) we observe distinct wave-packet collapse and fractional and full revival structures. Finally, Sec. IV gives a short summary.

II. MODEL SYSTEM

This section introduces the model trapped-ion Hamiltonian. The problem is first formulated in terms of operator algebra, commonly used in the quantum optics community, and then recast in the conjugate-variable representation frequently applied in, for instance, molecular physics. Within the latter representation, the Hamiltonian obtained resembles

that of an artificial diatomic molecule with two coupled bound electronic states. There are several parameters determining the particular form of the potential curves and coupling: namely, effective ion-laser coupling λ (Rabi frequency), trap frequency ω, laser frequency ω_L, ion transition frequency Ω, LD parameter (proportional to the laser wave number) η, and laser phase shift ϕ. For a large LD parameter, the curves exhibit several crossings, whereas for small η one may encounter only a few, one, or even no crossings in the parameter range of interest. We will here be interested exclusively in the situation of a single-level crossing of the two potential curves.

A. Trapped ion in a standing wave

In the formalism of phonon creation $\hat{a}^\dagger$ and annihilation $\hat{a}$ operators the Hamiltonian reads (we use atomic units so that $\hbar = 1$)

$$H = \omega \hat{a}^\dagger \hat{a} + \frac{\Delta}{2}\hat{\sigma}_z + \lambda \, \cos[\eta(\hat{a}^\dagger + \hat{a}) + \phi]\hat{\sigma}_x, \qquad (1)$$

with the ion-laser detuning $\Delta = \Omega - \omega_L$ and the $\hat{\sigma}$ operators act on the two ionic levels $|1\rangle$ and $|2\rangle$, $\hat{\sigma}_z = |2\rangle\langle 2| - |1\rangle\langle 1|$ and $\hat{\sigma}_x = |1\rangle\langle 2| + |2\rangle\langle 1|$. The LD parameter is defined in terms of the ionic mass m and laser wave number k as $\eta = k\sqrt{m\omega/2}$, and the relative position of the trap in the standing wave laser field is determined by ϕ.

In order to gain a deeper understanding of the evolution we discuss the approximations regularly applied in trapped-ion models. These often result in analytically solvable effective Hamiltonians. In the LD regime $\eta \ll 1$, we may expand the cosine function to obtain

$$H \approx \omega \hat{a}^\dagger \hat{a} + \frac{\Delta}{2}\hat{\sigma}_z + \lambda[\cos(\phi) - \eta \sin(\phi)(\hat{a}^\dagger + \hat{a})]\hat{\sigma}_x + O(\eta^2). \qquad (2)$$

In this regime, the effect of the phase shift ϕ is clear. For $\phi = k\pi$, where k is an integer, the ionic vibrational states are not coupled by the external laser (*carrier pumping*), whereas if $k = 1/2, 3/2, \ldots$, the vibrational states do couple (*sideband pumping*) [38]. In the latter case, the Hamiltonian (2) coincides with the Rabi model [28]. Neglecting the virtual processes (i.e., $\hat{a}\hat{\sigma}^-$ and $\hat{a}^\dagger\hat{\sigma}^+$ corresponding to simultaneous de-excitation or excitation of the field and the ion) one derives the regular JC Hamiltonian in the RWA:

$$H_{JC} = \omega \hat{a}^\dagger \hat{a} + \frac{\Delta}{2}\hat{\sigma}_z + g(\hat{a}^\dagger\hat{\sigma}^- + \hat{\sigma}^+\hat{a}), \qquad (3)$$

where in this case $g = \lambda\eta$ and $\hat{\sigma}^+ = |2\rangle\langle 1|$ and $\hat{\sigma}^- = |1\rangle\langle 2|$. The JC model is analytically solvable, and the eigenvalues of its corresponding Hamiltonian are known as (up to an overall constant)

$$E_{JC}^\pm(n) = \omega n \pm \sqrt{\frac{(\Delta - \omega)^2}{4} + g^2 n}, \quad n = 0, 1, 2, \ldots . \qquad (4)$$

As pointed out, the effective RWA Hamiltonian, in principle, is only justified for $\cos(\phi) = 0$, whereas in general situations

more sophisticated RWA approaches must be considered. Turning to an interaction picture with respect to the free field and ion, the Hamiltonian (2) becomes

$$\begin{aligned}
H_I = U_I H U_I^{-1} = {}&\lambda \, \cos(\phi)(\hat{\sigma}^+ e^{-i\,\Delta t} + \hat{\sigma}^- e^{i\,\Delta t}) - \eta\lambda \, \sin(\phi) \\
&\times (\hat{a}^\dagger\hat{\sigma}^- e^{-i(\omega-\Delta)t} + \hat{\sigma}^+\hat{a} \, e^{i(\omega-\Delta)t}) - \eta\lambda \, \sin(\phi) \\
&\times (\hat{a}^\dagger\hat{\sigma}^- e^{-i(\omega+\Delta)t} + \hat{\sigma}^+\hat{a} \, e^{i(\omega+\Delta)t}),
\end{aligned} \qquad (5)$$

where $U_I = \exp(-i\omega\hat{a}^\dagger\hat{a}t)\exp(-i\frac{\Delta}{2}\hat{\sigma}_z t)$. This introduces three different time scales of the interaction, suggesting an application of the RWA. It is known, however, that the validity of the RWA does not solely depend on the time scales involved, but also on the relative amplitudes of the coupling parameters [28,29]. In particular, only for ion-field couplings much smaller than the ion-level separation and vibrational spacing—$\lambda\eta\sin(\phi) \ll \Omega, \omega$ and $\lambda\cos(\phi) \ll \Omega, \omega$—is the RWA justified. We then note the following: First, the Lamb-Dicke regime seems to favor application of the RWA, which, in fact, we have verified by numerical calculation. Second, the angle ϕ is of importance for the validity of the RWA and together with the three characteristic time scales it becomes clear that a straightforward application of the RWA in the basis presented above is nontrivial. The first observation will be of importance further on when we introduce the adiabatic approximation. The second is indeed an interesting issue that was resolved by Wu and Yang [17]. Their idea is that also the third term of the expanded Hamiltonian (2) is considered as a "free" part and these first three terms define the interaction picture and the proper time scales. Within this frame, the slowly oscillating terms describe a JC type of interaction between the field (vibrations) and "dressed" atomic states [39] differing from the $|1\rangle$ and $|2\rangle$ states.

Yet another, but related, approach is to use the expansion [40,41]

$$\begin{aligned}
\cos[\eta(\hat{a}^\dagger + \hat{a}) + \phi] = {}&e^{-\eta^2/2}\sum_{k=0}^{\infty} \epsilon_k \frac{(-\eta)^k}{k!}\cos\left(\phi + k\frac{\pi}{2}\right) \\
&\times [\hat{a}^k f_k(\hat{n}+k) + f_k(\hat{n}+k)(\hat{a}^\dagger)^k],
\end{aligned} \qquad (6)$$

where

$$f_k(\hat{n}) = \sum_{m=0}^{\infty} \frac{(\hat{n}-m+1)_m}{(k+1)_m m!} = k! \, \frac{L_{\hat{n}}^k(\eta^2)}{(\hat{n}+1)_k}, \qquad (7)$$

with $(\hat{n}-m+1)_m = \hat{n}(\hat{n}-1)\cdots(\hat{n}-m+1)$, $\hat{n} = \hat{a}^\dagger\hat{a}$, $\epsilon_k = 1/2$ for $k = 0$ and $\epsilon_k = 1$ otherwise, and $L_{\hat{n}}^k(\eta^2)$ are the generalized Laguerre polynomials. Imposing suitable resonance conditions $(|\Delta - \omega| \ll |\Delta - k\omega|$ for $k = 0, 2, 3, 4, \ldots)$ between the constituting frequencies, we may for proper amplitudes of the couplings employ a RWA to regain a JC-like interaction in terms of "deformed" oscillator operators $\hat{A} = \hat{a}f_1(\hat{n}+1)$. The $\hat{A}$ and $\hat{A}^\dagger$ define generalized boson operators obeying modified boson algebras, and they specify, for instance, nonlinear Fock and coherent states being eigenstates of $\hat{A}^\dagger\hat{A}$ and $\hat{A}$, respectively. Note that, in some sense, the new ladder operators can

be viewed as describing a nonlinear oscillator with amplitude-dependent frequency. Additionally, it is known that the anharmonicity of an oscillator greatly affects physical phenomena like collapse and revivals [42]. Related algebraic techniques, in particular shape invariance and supersymmetry, can therefore be a useful tool for describing molecular dynamics where oscillators are in general anharmonic [43]. We remark, however, that most of these models [43] employ the standard RWA as it is used in the JC model, while it is clear that this is in general less justified than for the JC model, due to varying distance between energy eigenvalues, for instance.

We pointed out above that the relative size between the effective laser-ion coupling λ and the two-level spacing Ω is crucial for the validity of the RWA. Also the relation between λ and ω is important. In general, the strong-excitation regime [24] $\lambda \gg \omega$ invalidates the RWA and the LD approximation, while, for moderate phonon numbers ($n \lesssim 10$), the opposite weak-excitation regime [22] favors them. It should be emphasized, though, that, eventually, the applicability of the approximations depends on all parameters, including Ω and η, and their mutual relations.

Now, rather than by the boson creation and annihilation operators as above, we represent the Hamiltonian in terms of conjugate variables

$$\hat{x} = \sqrt{\frac{1}{2m\omega}}(\hat{a}^\dagger + \hat{a}),$$

$$\hat{p} = i\sqrt{\frac{m\omega}{2}}(\hat{a}^\dagger - \hat{a}), \qquad (8)$$

obeying the regular canonical commutator relation. In this nomenclature we find

$$H = \frac{\hat{p}^2}{2m} + \frac{m\omega^2}{2}\hat{x}^2 + \begin{bmatrix} \dfrac{\Delta}{2} & \lambda\cos(k\hat{x}+\phi) \\[2mm] \lambda\cos(k\hat{x}+\phi) & -\dfrac{\Delta}{2} \end{bmatrix}, \qquad (9)$$

where k is the external laser wave number and m the mass of the ion. This representation of the Hamiltonian serves as the starting point of our analysis; for a given initial state, its wave packet will evolve on two coupled harmonic oscillators according to Eq. (9). We note that in the x representation a *Fock state* of the vibrations, $\hat{n}|n\rangle = n|n\rangle$, or a *coherent state* $\hat{a}|\alpha\rangle = \alpha|\alpha\rangle$, reads

$$\varphi_n(x) = \langle x|n\rangle = \left(\frac{\sqrt{m\omega}}{2^n\sqrt{\pi}n!}\right)^{1/2} H_n(\sqrt{m\omega}x)e^{-m\omega x^2/2},$$

$$\varphi_\alpha(x) = \langle x|\alpha\rangle = \left(\frac{m\omega}{\pi}\right)^{1/4} e^{[\mathrm{Im}(\alpha)]^2}e^{-m\omega[x-(\sqrt{2/m\omega})\alpha]^2/2}. \qquad (10)$$

Here, $H_n(x)$ is the nth Hermite polynomial.

B. Base representations

To gain a deeper intuition of the problem it is in order to discuss the various bases that will be used in the following. One natural representation is that of *bare basis states*, which are the eigenstates of the free Hamiltonian part $\{|n,1\rangle, |n,2\rangle\}$, where n represents the nth Fock eigenstate of the harmonic oscillator. In x representation the bare basis states are written as

$$\langle x|n,1\rangle = \varphi_n(x)\begin{bmatrix}1\\0\end{bmatrix}, \quad \langle x|n,2\rangle = \varphi_n(x)\begin{bmatrix}0\\1\end{bmatrix}.$$

A general *bare state* is given by $\psi_1(x)|1\rangle$ or $\psi_2(x)|2\rangle$ for some normalized wave function $\psi_i(x)$. From the form in which the Hamiltonian (9) is presented, it is clear that the external laser field enters in the off-diagonal terms and hence couples these states. The bare states can be used to define *bare potential curves* as the diagonal potential elements of the Hamiltonian in the ionic basis, $|1\rangle$ and $|2\rangle$. Thus, the bare potentials are two centered oscillators shifted in energy with either $\Delta/2$ or $-\Delta/2$.

The eigenstates of the full Hamiltonian are called *dressed basis states* and denoted by $|\chi_n^+\rangle$ and $|\chi_n^-\rangle$. We have introduced the superscript $\pm$ since, for a wide range of parameters, the eigenstates come in pairs, which is true in particular when the RWA or the LD approximation or both have been imposed, as seen in (4) for the JC model. In these regimes, not necessarily only for the JC model, "simple" analytic solutions to the problem are available, whereas in the general case this is not true. Note that there is no obvious corresponding set of dressed potential curves.

The above two bases are part of the conventional terminology of quantum optics. We now turn to a more convenient representation of coupled molecular electronic states. For this purpose, we employ the x representation and rotate the Hamiltonian (9) around the $(\hat{\sigma}_x + \hat{\sigma}_z)$ axis by the unitary operator $U_1 = \frac{1}{\sqrt{2}}(\hat{\sigma}_x + \hat{\sigma}_z)$, giving

$$\tilde{H}_1 = U_1 H U_1^{-1} = \frac{\hat{p}^2}{2m} + \frac{m\omega^2}{2}\hat{x}^2$$

$$+ \begin{bmatrix} \lambda\cos(k\hat{x}+\phi) & \dfrac{\Delta}{2} \\[2mm] \dfrac{\Delta}{2} & -\lambda\cos(k\hat{x}+\phi) \end{bmatrix}. \qquad (11)$$

This transformation swaps the off-diagonal terms with the diagonal ones of the last term in the Hamiltonian. The form of $\tilde{H}_1$ has many similarities with the Hamiltonian describing a diatomic molecule in a diabatic representation. The off-diagonal elements in (11) are in potential form; i.e., they do not contain differential operators. Here, the couplings are $\hat{x}$ independent, which, however, is also frequently assumed in models used in molecular physics—e.g., the Landau-Zener model [44]. Note that in our ion-trap system $\hat{x}$ represents the spatial center-of-mass position of the ion in the trap, whereas in the molecular counterpart $\hat{x}$ is the internuclear distance. The operator U_1 transforms the bare internal ionic states as

TABLE I. States and potentials used in this article. Here, $i=1,2$ and $\psi_i(x)$ is a general normalized wave function.

State	Definition	Potentials
Bare	$\psi_i(x)|i\rangle$	$V^B_\pm(\hat{x}) = \frac{m\omega^2}{2}\hat{x}^2 \pm \frac{\Delta}{2}$
Dressed	Eigenstates of full Hamiltonian (9), $|\chi_n^\pm\rangle$	
Diabatic	$\psi_-(x)|-\rangle = \psi_-(x)U_1|1\rangle, \quad \psi_+(x)|+\rangle = \psi_+(x)U_1|2\rangle$	$V^D_\pm(\hat{x}) = \frac{m\omega^2}{2}\hat{x}^2 \pm \lambda\cos(k\hat{x}+\phi)$
Adiabatic	$\psi_i(x)|i\rangle_{ad} = \psi_i(x)U_2|i\rangle$	$V^A_\pm(\hat{x}) = \frac{m\omega^2}{2}\hat{x}^2 \pm \varepsilon(\hat{x})$

$$|-\rangle = U_1|1\rangle = \frac{1}{\sqrt{2}}\begin{bmatrix} 1 \\ 1 \end{bmatrix},$$

$$|+\rangle = U_1|2\rangle = \frac{1}{\sqrt{2}}\begin{bmatrix} 1 \\ -1 \end{bmatrix}, \tag{12}$$

which defines the *diabatic states* as $\langle x|\psi_\pm\rangle|\pm\rangle = \psi_\pm(x)|\pm\rangle$ and the corresponding *diabatic potential curves* as the diagonal potential matrix terms of (11). Thus, contrary to the bare curves, these are centered oscillators modified by $\pm\lambda\cos(k\hat{x}+\phi)$ and depending on the parameter amplitudes very different types of diabatic potentials may be obtained. For example, if the oscillating cosine function dominates over the harmonic oscillator (in the spatial range of interest), the system is semiperiodic and is best understood from Bloch or Floquet theory [46]. In the opposite limit of a small λ and k we may expand the cosine as in (2) to find the two centered oscillators both shifted and displaced according to the added terms $\pm\lambda[\cos(\phi) - \eta\sin(\phi)\hat{x}]$. In this paper, we are interested in a regime intermediate between the two.

Given a Hamiltonian in the form of (9), the transformation

$$U_2 = \begin{bmatrix} \cos(\theta) & -\sin(\theta) \\ \sin(\theta) & \cos(\theta) \end{bmatrix}, \tag{13}$$

with

$$\tan(2\theta) = \frac{2\lambda\cos(k\hat{x}+\phi)}{\Delta}, \tag{14}$$

diagonalizes the last term of the Hamiltonian. However, since U_2 is $\hat{x}$ dependent, it does not commute with $\hat{p}$ and explicitly we get

$$\tilde{H}_2 = U_2 H U_2^{-1} = \frac{\hat{p}^2}{2m} + \frac{m\omega^2}{2}\hat{x}^2 + (\partial\theta)^2$$
$$+ \begin{bmatrix} \varepsilon(\hat{x}) & \partial^2\theta - 2i(\partial\theta)\hat{p} \\ -\partial^2\theta + 2i(\partial\theta)\hat{p} & -\varepsilon(\hat{x}) \end{bmatrix}, \tag{15}$$

where $\partial f \equiv \partial f/\partial x$ and

$$\varepsilon(\hat{x}) = \sqrt{\Delta^2/4 + \lambda^2\cos^2(k\hat{x}+\phi)}. \tag{16}$$

These diagonal terms, neglecting the *centrifugal term* $(\partial\theta)^2$ [45], define the *adiabatic potential curves*, while U_2 acting on the bare states gives the *adiabatic states* $\langle x|\psi\rangle|i\rangle_{ad} = \psi(x)|i\rangle_{ad} = \psi(x)U_2|i\rangle$ for $i=1,2$. Note that $|i\rangle_{ad}$ is in general x dependent. The diagonal and nondiagonal terms containing $\partial\theta$ and $\partial^2\theta$ are the nonadiabatic corrections, and if these play a minor role in the wave-packet evolution, the dynamics is said to be adiabatic. For the present system, we have

$$\partial\theta = -\frac{\Delta k\lambda s}{\Delta^2 + \lambda 2c^2},$$

$$\partial^2\theta = -\frac{\Delta[\lambda k^2 c(\Delta^2 + 4\lambda^2 c^2) - 8\lambda^3 k^2 cs^2]}{(\Delta^2 + 4\lambda^2 c^2)^2}, \tag{17}$$

where $s=\sin(k\hat{x}+\phi)$ and $c=\cos(k\hat{x}+\phi)$, and typically the second, higher-derivative term is smaller. For diatomic molecules an equivalent transformation from the diabatic to an adiabatic representation can be applied. Consequently, also then nonadiabatic couplings are both $\hat{x}$ and $\hat{p}$ dependent. We recall, as discussed in the previous section, that the RWA and the LD approximation are highly related in terms of validity ranges and especially $\eta \ll 1$ (or likewise for small k) is a constraint on their implementation. Here, as well, we note that for small k the nonadiabatic coupling terms (17) become small. On top, we claimed that $\lambda < \Delta$ is also a condition for the applicability of the RWA and the LD approximation, which from (17) again is seen to favor the adiabaticity. We have verified by numerical calculation that all three approximations more or less share the same parameter validity range. From (17) one notes that also the case when $\Delta \equiv 0$ gives vanishing nonadiabatic corrections. This limit, however, does not represent a proper adiabatic one, but rather the diabatic limit, and is hence sometimes referred to as the antiadiabatic limit. Since we consider parameters where the adiabatic approximation breaks down, it follows that we can apply neither the RWA nor the LD approximation.

In Table I, we summarize the various bases, while in Fig. 2 we show some typical examples of the corresponding potentials. Note that at the crossing point, when the cosine function is zero, the bare and adiabatic potentials coincide, while away from the crossing the diabatic and adiabatic curves approach each other for the current set of parameters. We may point out that different definitions of the above bases exist, and in particular in quantum optics is the bare-diabatic and the dressed-adiabatic representations often iden-
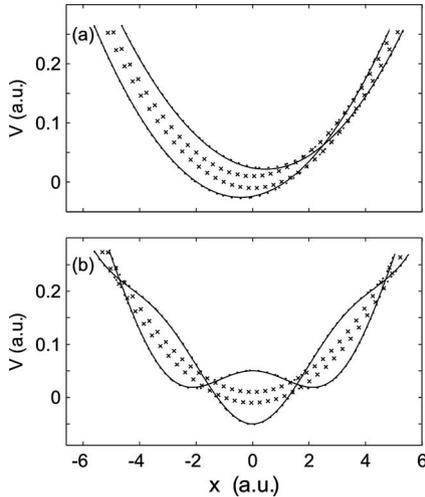
FIG. 2. Example potentials: bare (crosses), diabatic (solid line), and adiabatic (dots). In (a), the potentials only possess one crossing in the shown interval, while (b) displays an example of several crossings. The parameters (in atomic units) are $m = 80\,000$, $\omega = 0.0005$, $\lambda = 0.05$, and $\Delta = 0.02514$ in both plots, while $k = 0.2$ and $\phi = 1.072\,490\,74$ rad in (a) $k = 1$ and $\phi = 0$ rad in (b).

tical. Identifying bare states as diabatic ones and dressed states with adiabatic ones does not, however, properly coincide with the common definitions in molecular and chemical physics. Adiabatic states are in general not eigenstates of the full Hamiltonian, as dressed states are, and diabatic states usually approximate the adiabatic ones far from curve crossing regions, which is not the case of bare states.

III. DYNAMICS: BISTABLE MOTION

The existence of bistable evolution is a direct consequence of interference between the constituent wave-packet parts, as shown in Fig. 1. The bistable motion turns out to be stable over very long time periods, showing clear oscillations, collapses, and revivals [36]. In order for the wave-packet fractions to overlap and interfere correctly, a necessary, but not sufficient, condition for bistable motion is that the two parts of the split wave packet should return simultaneously to the starting point. We denote this period of time by T_{cl}, where the index cl stands for classical, and it is determined from the first maximum of the autocorrelation function, as will be described below. Further, let $P_i(t)$ be the population in the diabatic state $|i\rangle$ (we hence trace out the field degrees of freedom). If, initially, the wave packet is in the diabatic state i, we define $P_{sp} = 1 - P_i(t = T_{cl}/2)$, which gives the population in the opposite diabatic state at half a classical period. In other words, P_{sp} in a sense measures the amount of splitting of the wave packet as it traverses the crossing and, hence, for times shorter than the collapse time $P_i(jT_{cl}) \approx 1$ ($j = 0, 1, 2, \ldots$) for a bistable trajectory. Naturally, $0 \leq P_{sp} \leq 1$, where $P_{sp} = 0$ corresponds to diabatic and $P_{sp} = 1$ to adiabatic evolution, and in particular, bistable trajectories are not restricted to a certain P_{sp}. It is clear, however, that for the nontrivial intermediate values of P_{sp}, these types of interferences are sensitive to parameter values. In

addition to bistable trajectories, the parameters may be tuned so that $P_i((2j+1)T_{cl}) \approx 0$ and $P_i(2jT_{cl}) \approx 1$, where again $j = 0, 1, 2, \ldots$, which defines an *astable trajectory*. Here, however, we focus on the more stable bistable case.

For a general set of bound coupled (or uncoupled) potential curves we may expand the eigenenergies around the mean set of quantum numbers n_0 forming the wave packet. For a single discrete number n this reads

$$E(n) \approx E(n_0) + E'(n_0)(n - n_0) + \frac{E''(n_0)}{2}(n - n_0)^2$$

$$+ \frac{E'''(n_0)}{6}(n - n_0)^3 + \cdots, \quad (18)$$

where $E'(n_0) = [dE(n)/dn]_{n=n_0}$, and so forth, and $n_0 \gg 1$ is the "average" quantum number of the wave packet. The wave packet is assumed to be composed of eigenstates with quantum numbers n fairly localized around n_0. We define the different time scales

$$T_{cl} = \frac{2\pi}{|E'(n_0)|}, \quad T_{rev} = \frac{2\pi}{|E''(n_0)|/2}, \quad T_{sup} = \frac{2\pi}{|E'''(n_0)|/6},$$

$$(19)$$

characterizing the *classical vibration*, *revival*, and *superrevival* time, respectively. Note that for a single harmonic oscillator $T_{cl} = 2\pi/\omega$ and the higher-order terms vanish, which is equivalent to letting the latter characteristic time scales go to infinity. For two uncoupled different harmonic oscillators 1 and 2 one has the respective classical periods $T_{cl}^{(1)} = 2\pi/\omega_1$ and $T_{cl}^{(2)} = 2\pi/\omega_2$, where ω_i is the frequency of the oscillator i. The combined classical period becomes $T_{cl} = T_{cl}^{(1)}k = T_{cl}^{(2)}l$, where k and l are the smallest possible integers obeying the condition $k\omega_2 = l\omega_1$. Thus, it is clear that for multilevel systems the typical time scales can be very long. As an example, returning to the JC model (4), the revival time is usually defined in the quantum optics community as the time it takes for the constituent neighboring Rabi frequencies $\Omega_n = \sqrt{(\Delta - \omega)^2/4 + g^2 n}$ to differ by π[50]:

$$(\Omega_{n_0+1} - \Omega_{n_0})T_{rev} = \pi. \quad (20)$$

Consequently, the JC revival time as it is given in (20) is more reminiscent of the classical period rather than the revival one according to the definition (19). Also the fractional and superrevivals as discussed in the literature of the JC model differ from the ones of Eq. (19); see [47].

The wave-packet propagation is carried out using the Chebychev polynomial method [48]. We assume the initial state to be of the form $\psi(x,0)|+\rangle$, where $\psi(x,0)$ is taken to be a minimum uncertainty Gaussian function

$$\Psi(x,0) = \psi(x,0)|+\rangle = \left(\frac{1}{2\pi\sigma^2}\right)^{1/4} e^{-(x-x_0)^2/4\sigma^2}, \quad (21)$$

including also the case of coherent states. This wave packet is let to evolve over long time periods, typically T_{rev}. The quantities of interest for us are

$$W(t) = \langle \hat{\sigma}_z \rangle, \quad \text{inversion,}$$

$$A(t) = \int \left[\Psi^*(x,t)\Psi(x,0) dx \right], \quad \text{autocorrelation,}$$

$$S_I(t) = -\text{Tr}[\rho_I \ln(\rho_I)], \quad \text{entropy,} \qquad (22)$$

where $\Psi(x,t)$ is the full two-level wave packet at time t and $\rho_I = \text{Tr}_F[\rho]$ is the reduced density operator for the ion, obtained once the field degrees of freedom of the full density operator $\rho = |\Psi(x,t)\rangle\langle\Psi(x,t)|$ have been traced out. Note that $W(t)$ is the inversion between the bare states $|2\rangle$ and $|1\rangle$. The autocorrelation function determines the overlap between the initial state with the one at time t, while the *von Neumann entropy* is a measure of the degree of entanglement shared between the field and the ion. For initial pure states, as in our case, the entropy is the same for the field and the ion: $S_I(t) = S_F(t)$ [49]. An advantage of our numerical wave-packet approach is that, once the full wave packet $\Psi(x,t)$ is given, all the above quantities are easily calculated, as well as other relevant properties.

A. Short-time evolution

By short times we refer to time scales of order $T_{cl} \ll T_{rev}$ corresponding to a single or few oscillations of the total wave packet. We tune the parameters to have 50:50 splitting of the wave packet at the curve crossing—i.e., $P_{sp} = 1/2$—corresponding to maximal entanglement. The initial wave packet is localized around $\alpha = x_0\sqrt{m\omega}/\sqrt{2} = 6\sqrt{m\omega}/\sqrt{2} \approx 26.8$ for the considered mass, and thus for the chosen parameters the motion is highly excited with a mean phonon vibrational number $n_0 = 720$. Its width is either $\sigma = 0.047$ (highly squeezed [51]) or we pick σ as for a coherent state with given mass m. In atomic units, $m = 80\,000$, which corresponds to 42 amu. The results are applicable to any mass, however, provided the time is scaled accordingly. The rest of the parameters are as in Fig. 2(a), except Δ that should be divided by 5.

In Fig. 3 we display the numerical results of the quantities (22); (a)–(c) refer to an initial coherent state and (d)–(f) an initial Gaussian distribution with $\sigma = 0.047$. We note that in both cases almost perfect 50:50 splitting is obtained, and thus the system is maximally entangled on one side of the level crossing, while it is disentangled on the opposite side. The state can be written as

$$\Psi(x,t) = \psi_+(x,t)|+\rangle + \psi_-(x,t)|-\rangle = \frac{1}{\sqrt{2}}[\psi_-(x,t) + \psi_+(x,t)]|1\rangle$$

$$+ \frac{1}{\sqrt{2}}[\psi_-(x,t) - \psi_+(x,t)]|2\rangle. \qquad (23)$$

For 50:50 splitting and well-separated split wave packets, we have that the vibrational wave functions of the bare states, $|1\rangle$ and $|2\rangle$, are orthogonal, in agreement with the maximal entanglement. At this instant, the combined bipartite ion-phonon system is in an Einstein-Podolsky-Rosen (EPR) Schrödinger cat state. To a first approximation, we may assume the wave packets to keep their shape over a time period of one classical oscillation. That is, for initial coherent states, the split states are still coherent with modulated phase and amplitude. This is indeed verified below, where we consider the dynamics in phase space. Thus, the phonon distributions in this case are Poissonians for the diabatic states, while for the bare states they would be made out of the sum of two coherent states with equal phase but different amplitudes.

FIG. 3. Inversion $W(t)$, autocorrelation $A(t)$, and entropy $S_I(t)$ for a coherent (a)–(c) and a squeezed (d)–(f) initial state. See text for the parameters.

Calculating the variance of the wave packets, one notes that the squeezed state [51] $\sigma = 0.047$ shows typical breathing motion while traversing the potential back and forth. From the decrease in amplitudes, the quantities corresponding to the coherent state are seen to be more sensitive than for the squeezed state, or in other words, the collapse time is faster. This fast dephasing comes about due to the larger spread in phonon numbers n for the coherent initial state. It also shows up as rapid oscillations in the inversion around the curve crossings.

The plots also give a measure of the characteristic transition time at the level crossing [52], and one notes that this time is rather short compared to the full time T_{cl}, which is indeed known from other similar models [53]. Interestingly, we have found that a short crossing time as well as the sharp peaks with large amplitudes in the inversions, (a) and (d), around the crossings are typical for the bistable cases. The bare-state inversion can be expressed in terms of the diabatic wave packets as $\langle \hat{\sigma}_z \rangle = 2\text{Re}[\int \psi_+^*(x,t)\psi_-(x,t)dx]$ and is hence related to the coherence of diabatic wave packets. We note that the total energy can be written as

$$E_{tot}(t) = \sum_{i=+,-} \int \psi_i^*(x,t)H_{ii}\psi_i(x,t)dx + \frac{\Delta}{2}W(t), \qquad (24)$$

where H_{++} and H_{--} are two diagonal matrix elements of the Hamiltonian (11). From this it is seen that the bare state inversion is a measure of the diabatic energy transfer.

At first, it may seem surprising that the inversion $W(t)$ can be nonzero at the right side of the crossing, even if the autocorrelation $A(t)$ is close to 1 and the entropy $S_I(t)$ is close to zero. The zero entropy, however, is not a contradiction as the field and ion states can be separated, provided the constituent wave packets fractions $\psi_+(x,t)$ and $\psi_-(x,t)$ differ merely by a complex constant. For the inversion we have

$$W(t) = \langle \psi_2(t) | \psi_2(t) \rangle - \langle \psi_1(t) | \psi_1(t) \rangle = 2\mathrm{Re}[\langle \psi_+(t) | \psi_-(t) \rangle]$$
$$\leq 2\sqrt{[1 - \langle \psi_-(t) | \psi_-(t) \rangle] \langle \psi_-(t) | \psi_-(t) \rangle}, \quad (25)$$

while for the autocorrelation

$$|A(t)|^2 = |\langle \Psi(t) | \Psi(0) \rangle|^2 = |\langle \psi_+(t) | \psi_+(0) \rangle|^2 \leq 1 - \langle \psi_-(t) | \psi_-(t) \rangle. \quad (26)$$

For sufficiently small $\langle \psi_-(t) | \psi_-(t) \rangle$ it follows that $A(t)$ can be close to 1 even if $W(t)$ is not exactly zero.

The wave-packet splitting manifests itself also in the phase-space distributions [28]. In Fig. 4 we display snapshots of the Wigner distribution [54]

$$\mathcal{W}(p,x) = \frac{1}{(2\pi)^2} \int d\xi \int d\tau \, e^{i(\tau p + \xi x)} \mathrm{Tr}_I[e^{-i(\tau p + \xi x)}\rho]$$
$$= \frac{1}{\pi} \int dy \, e^{-i2py}[\psi_+^*(x-y)\psi_+(x+y)$$
$$+ \psi_-^*(x-y)\psi_-(x+y)] \quad (27)$$

over one period of oscillation for a coherent state (a) and a close-up at the Wigner distribution close to half an oscillation for a coherent (b) and squeezed (c) state. In (d) we show the Wigner distribution after the collapse at approximately $t \approx 2000 T_{cl}$ for a squeezed state. The spreading of the distribution over the whole accessible phase-space is a character of the collapse. At times of fractional revivals, the wave packet forms multiple localized bumps [55]. The two constituent parts of $\mathcal{W}(p,x)$ for short times approximately follow the "classical" phase-space trajectories

$$\frac{\partial x_c}{\partial t} = \frac{\partial H^{(i)}}{\partial p_c}, \quad \frac{\partial p_c}{\partial t} = -\frac{\partial H^{(i)}}{\partial x_c}, \quad (28)$$

with the adiabatic and diabatic Hamiltonians $H^{(i)} = \frac{p_c^2}{2m} + V^{(i)}(x)$ and $i = A, D$. The small anharmonicity of the potentials is reflected in the pattern of the Wigner distribution. The squeezed distributions rotate along the trajectories, which gives rise to the characteristic breathing motion of its width. The phase-space plots suggest that the two involved wave packets roughly evolve on either of the potential curve $V_-^D(x)$ or $V_+^A(x)$, and at the right side away from the crossing point these two approximately coincide. We argued that the corresponding classical times must be equal, $T_{cl}^{A+} = T_{cl}^{D-}$, in order for the wave packets to overlap at the curve crossing and interfere maximally. This, however, does not imply that the longer time scales $T_{rev}^A, T_{rev}^D, T_{sup}^A, \ldots$ of the potentials are equal, as will be discussed next.
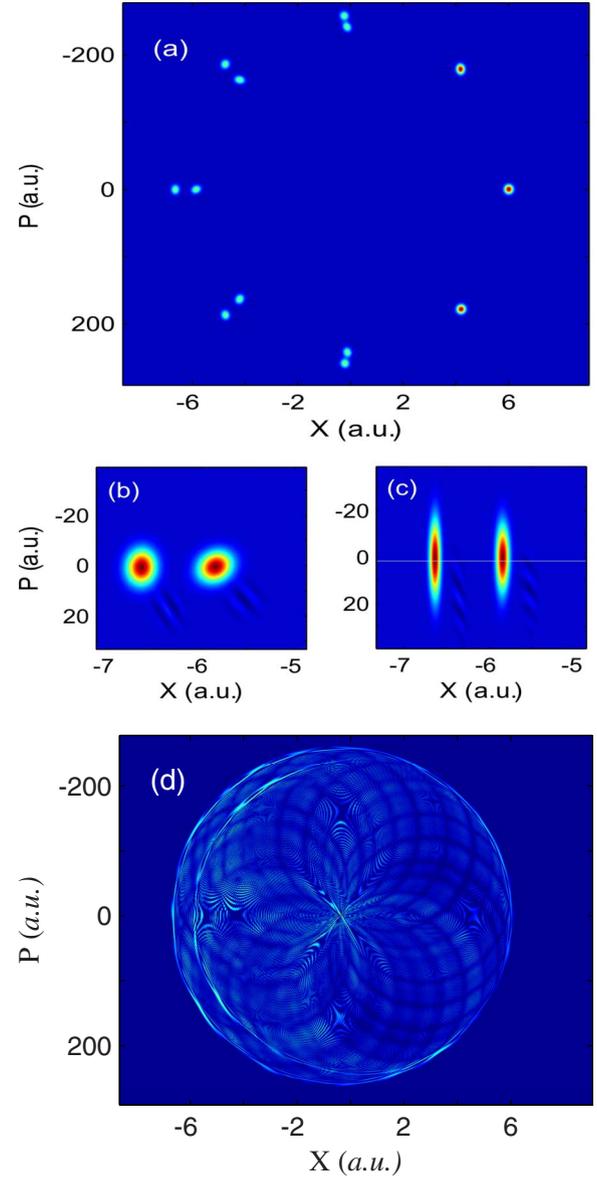
FIG. 4. (Color online) The Wigner distribution for an initial coherent state (a) and (b) and for a squeezed state (c) and (d). The first plot shows snapshots throughout one period of oscillation, while (b) and (c) zooms in at the distributions around half oscillation time. In (d) the distribution at the time of collapse is displayed.

B. Long-time evolution

We now turn to the dynamics over time scales of the order of T_{rev}, which for our parameters correspond to several thousands of classical oscillations. Since we consider situations of large phonon excitations, this does not, however, necessarily imply exceedingly long total operational times.

The expansion of the eigenvalues (18), in general, contains an infinite number of terms, but for relatively smooth potentials one expects fairly fast convergence. Higher-order terms typically cause imperfect full-time and fractional revivals, by which we mean that the amplitude of, say, the autocorrelation function squared does not reach the values $1/j$, where $j = 1, 2, 3, \ldots$, as expected [42] for rational frac-
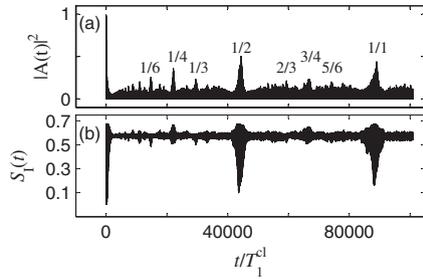
FIG. 5. Autocorrelation function (a) and von Neumann entropy (b) for an initial squeezed state in the case of 40:60 splitting.

tions of the revival time kT_{rev}/j, k and j mutually prime. This effect, arising from higher-order anharmonicities, is naturally more pronounced for longer times, and hence the revival amplitudes drop for each consecutive revival period T_{rev}. The widths of the revival peaks are getting broader, as well. As seen in Fig. 3, the uncertainty in phonon numbers n affects the collapse-revival pattern. In particular, the envelope functions of the revival peaks are highly sensitive to the uncertainty Δn, while the locations of the peaks are determined by the average n_0. In the "ideal" case, full amplitude revivals occur at $t=jT_{rev}/2$ for integer j, half amplitude revivals at $t=(2j+1)T_{rev}/4$, and so forth. In Fig. 5 we present the autocorrelation function (a) and von Neumann entropy (b) for a time span slightly longer than T_{rev}. The parameters and initial conditions are similar to the ones of Figs. 3(d)–3(f): ϕ = 1.072 440 805 316 56 rad, λ=0.064 727 653 164 347, σ =0.034 099 965 9, and Δ=0.005 025 343 787 836. The slight change in parameters gives 40:60 splitting (P_{sp}=0.4) rather than 50:50. Some of the numerous fractional revivals are labeled conventionally [42]. From Fig. 5(b), we note that in the collapse region the field and ion are highly entangled, but the fact that P_{sp}=0.4 causes a decrease of entanglement compared to the P_{sp}=1/2 case.

We have previously [36] studied the bistable motion and long-term revivals in system Hamiltonians with more resemblance to molecular models. In terms of the classical period, the revival time found in the present study is much longer than those we calculated for the molecular systems. This originates in a smaller anharmonicity of the ion-trap system. In [36], we found that in accordance with expectations from a semiclassical derivation the revival time of the coupled system, T_{rev}, can be obtained from the revival times of the adiabatic, $T_{rev}^{A_+}$, and diabatic, $T_{rev}^{D_-}$, pathways and the wave-packet splitting as

$$\frac{1}{T_{rev}} = \frac{P_{sp}}{T_{rev}^{A_+}} + \frac{1-P_{sp}}{T_{rev}^{D_-}}. \qquad (29)$$

This relation was fulfilled for numerous systems, comprising both coupled bound-bound and bound-repulsive states. Equation (29) accurately reproduces the limiting cases of adiabatic P_{sp}=1 and the diabatic P_{sp}=0 evolution. If $T_{rev}^{A_+} \neq T_{rev}^{D_-}$, then we presumably have that the size of T_{rev} is between the values of $T_{rev}^{A_+}$ and $T_{rev}^{D_-}$ in the intermediate range. However, in reality $T_{rev}^{A_+}$, $T_{rev}^{D_-}$, and P_{sp} are not independent variables as they all depend on the system parameters in a complex manner. To conclude, the revival time for multilevel systems can be shorter than those of individual isolated systems. For the classical periods, on the other hand, we found that $T_{cl}=T_{cl}^{A_+}$ =$T_{cl}^{D_-}$ for bistable trajectories. Thus, the dynamics cannot be viewed as two uncoupled wave packets evolving on the potential curves $V_+^A(x)$ and $V_-^D(x)$. Only interference between these two wave packets can cause a common revival time T_{rev} shorter than $T_{rev}^{A_+}$ or $T_{rev}^{D_-}$.

IV. CONCLUSION

In this article we have studied in a nonstandard way the dynamics of a harmonically trapped ion pumped by a standing wave beyond the RWA and the LD approximation. Using a wave-packet technique, we predict the existence of bistable states of motion similar to those observed for molecular systems [33–36]. These arise from interference of wave packets, and hence it is a pure quantum effect. Over longer time periods these states possess a well-resolved collapse-revival pattern including full and fractional revivals.

Beyond the conjecture of the new class of bistable ion-trap states, the article establishes a link between trapped-ion systems and molecular physics models. As such, we have put extra stress on how the two areas relate to one another: expressing the model Hamiltonian in x representation and introducing diabatic and adiabatic states and potential curves. We intend to further investigate these directions, both by considering algebraic methods in simple molecular models and by extending the current ion-trap system to include additional ionic internal levels and vibrational degrees of freedom. We will also allow for different trapping potentials in order to more closely mimic molecularlike situations. Anharmonic traps have been discussed in the literature, and then mainly quadrupole trapping [56], but in principle more exotic shapes may be gained by reforming and adjusting the geometry of the trap electrodes. Individual trapping potentials for the internal ionic levels have also been discussed [7].

[1] D. J. Wineland, C. Monroe, W. M. Itano, D. Leibfried, B. E. King, and D. M. Meekhof, J. Res. Natl. Inst. Stand. Technol. **103**, 259 (1998); D. Leibfried, R. Blatt, C. Monroe, and D. Wineland, Rev. Mod. Phys. **75**, 281 (2003); W. P. Schleich, *Quantum Optics in Phase Space* (Wiley, Berlin, 2001); W. P. Schleich, in *Quantum Entanglement and Information Processing*, edited by D. Esteve, J.-M. Raimond, and J. Dalibard (Elsevier, Amsterdam, 2004); S. Haroche and J. M. Raimond, *Exploring the Quantum* (Oxford University Press, Oxford, 2006).

[2] J. I. Cirac, A. S. Parkins, R. Blatt, and P. Zoller, Adv. At., Mol., Opt. Phys. **37**, 237 (1996).

[3] D. M. Meekhof, C. Monroe, B. E. King, W. M. Itano, and D. J. Wineland, Phys. Rev. Lett. **76**, 1796 (1996).

[4] S. Gulde, M. Riebe, G. P. T. Lancaster, C. Becher, J. Eschner, H. Haffner, F. Schmidt-Kaler, I. L. Chuang, and R. Blatt, Nature (London) **421**, 48 (2003); D. Leibfried, B. DeMarco, V. Meyer, D. Lucas, M. Barrett, J. Britton, W. M. Itano, B. Jelenkovic, C. Langer, T. Rosenband, and D. J. Wineland, *ibid.* **422**, 412 (2003); M. Riebe, H. Haffner, C. F. Roos, W. Hansel, J. Benhelm, G. P. T. Lancaster, T. W. Korber, C. Becher, F. Schmidt-Kaler, D. F. V. James, and R. Blatt, *ibid.* **429**, 734 (2004); M. D. Barrett, J. Chiaverini, T. Schaetz, J. Britton, W. M. Itano, J. D. Jost, E. Knill, C. Langer, D. Leibfried, R. Ozeri, and D. J. Wineland, *ibid.* **429**, 737 (2004).

[5] M. J. McDonnell, J. P. Home, D. M. Lucas, G. Imreh, B. C. Keitch, D. J. Szwer, N. R. Thomas, S. C. Webster, D. N. Stacey, and A. M. Steane, Phys. Rev. Lett. **98**, 063603 (2007).

[6] H. Moya-Cessa, A. Vidiella-Barranco, J. A. Roversi, D. S. Freitas, and S. M. Dutra, Phys. Rev. A **59**, 2518 (1999); H. Moya-Cessa, D. Jonathan, and P. L. Knight, J. Mod. Opt. **50**, 265 (2003).

[7] Ö. E. Müstecaphoglu and L. You, Phys. Rev. A **65**, 033412 (2002).

[8] A. B. Mundt, A. Kreuter, C. Becher, D. Leibfried, J. Eschner, F. Schmidt-Kaler, and R. Blatt, Phys. Rev. Lett. **89**, 103001 (2002).

[9] J. I. Cirac, A. S. Parkins, R. Blatt, and P. Zoller, Opt. Commun. **97**, 353 (1993); V. Buzek, G. Drobny, M. S. Kim, G. Adam, and P. L. Knight, Phys. Rev. A **56**, 2352 (1997); X. B. Zou, K. Pahlke, and W. Mathis, *ibid.* **65**, 064303 (2002).

[10] P. Treutlein, D. Hunger, S. Camerer, T. W. Hänsch, and J. Reichel, Phys. Rev. Lett. **99**, 140403 (2007); Y. Colombe, T. Steinmetz, G. Dubois, F. Linke, D. Hunger, and J. Reichel, Nature (London) **450**, 272 (2007); F. Brennecke, T. Donner, S. Ritter, T. Bourdel, M. Köhn, and T. Esslinger, *ibid.* **450**, 268 (2007); S. Slama, G. Krenz, S. Bux, C. Zimmermann, and P. W. Courteille, Phys. Rev. A **75**, 063620 (2007).

[11] B. M. Rodriguez-Lara, H. Moya-Cessa, and A. B. Klimov, Phys. Rev. A **71**, 023811 (2005).

[12] J. I. Cirac, A. S. Parkins, R. Blatt, and P. Zoller, Phys. Rev. Lett. **70**, 556 (1993); C. C. Gerry, Phys. Rev. A **55**, 2478 (1997).

[13] L. X. Li and G.-C. Guo, J. Opt. B: Quantum Semiclassical Opt. **1**, 339 (1999).

[14] J. I. Cirac, R. Blatt, A. S. Parkins, and P. Zoller, Phys. Rev. A **49**, 1202 (1994); M. F. Fang, S. Swain, and P. Zhou, *ibid.* **63**, 013812 (2000); F. Mao-Fa, Chin. Phys. **11**, 1028 (2002).

[15] C. A. Blockley, D. F. Walls, and H. Risken, Europhys. Lett. **17**, 509 (1992).

[16] S. Wallentowitz and W. Vogel, Phys. Rev. Lett. **75**, 2932 (1995); C. D'Helon and G. J. Milburn, Phys. Rev. A **54**, R25 (1996); F. E. Harrison, A. S. Parkins, M. J. Collett, and D. F. Walls, *ibid.* **55**, 4412 (1997).

[17] Y. Wu and X. Yang, Phys. Rev. Lett. **78**, 3086 (1997).

[18] S. Wallentowitz, W. Vogel, and P. L. Knight, Phys. Rev. A **59**, 531 (1999); S. Wallentowitz and W. Vogel, *ibid.* **58**, 679 (1998).

[19] Q. Y. Yang, L. F. Wei, and L. E. Ding, J. Opt. B: Quantum Semiclassical Opt. **7**, 5 (2005).

[20] R. Blatt, J. I. Cirac, A. S. Parkins, and P. Zoller, Phys. Scr. **T59**, 294 (1995); R. L. de Matos Filho and W. Vogel, Phys. Rev. Lett. **76**, 608 (1996).

[21] L. F. Wei, Y. Liu, and F. Nori, Phys. Rev. A **70**, 063801 (2004).

[22] M. Feng, X. Zhu, X. Fang, M. Yan, and L. Shi, J. Phys. B **32**, 701 (1999).

[23] J. I. Cirac, R. Blatt, A. S. Parkins, and P. Zoller, Phys. Rev. Lett. **70**, 762 (1993).

[24] J. F. Poyatos, J. I. Cirac, R. Blatt, and P. Zoller, Phys. Rev. A **54**, 1532 (1996); S. B. Zheng, X. W. Zhu, and M. Feng, *ibid.* **62**, 033807 (2000).

[25] T. Liu, K. L. Wang, and M. Feng, J. Opt. B: Quantum Semiclassical Opt. **40**, 1967 (2007).

[26] S. B. Zheng, Phys. Lett. A **245**, 11 (1998).

[27] J. I. Cirac and P. Zoller, Phys. Rev. Lett. **74**, 4091 (1995); K. Mølmer and A. Sørensen, *ibid.* **82**, 1835 (1999); D. Jonathan, M. B. Plenio, and P. L. Knight, Phys. Rev. A **62**, 042307 (2000); J. I. Cirac and P. Zoller, Nature (London) **404**, 579 (2000); F. Mintert and C. Wunderlich, Phys. Rev. Lett. **87**, 257904 (2001).

[28] J. Larson, Phys. Scr. **76**, 146 (2007).

[29] J. Larson, J. Phys.: Conf. Ser. **99**, 012011 (2008).

[30] E. J. Heller, J. Chem. Phys. **62**, 1544 (1975).

[31] B. M. Garraway and K. A. Suominen, Rep. Prog. Phys. **58**, 365 (1995).

[32] H. Dietz and V. Engel, Chem. Phys. Lett. **255**, 258 (1996).

[33] B. Zhang, N. Gador, and T. Hansson, Phys. Rev. Lett. **91**, 173006 (2003).

[34] N. Gador, B. Zhang, H. O. Karlsson, and T. Hansson, Phys. Rev. A **70**, 033418 (2004).

[35] N. Gador, B. Zhang, and T. Hansson, Chem. Phys. Lett. **412**, 386 (2005).

[36] D. Wang, Å. Larson, H. O. Karlsson, and T. Hansson, Chem. Phys. Lett. **449**, 266 (2007).

[37] E. T. Jaynes and F. W. Cummings, Proc. IEEE **51**, 89 (1963); B. W. Shore and P. L. Knight, J. Mod. Opt. **40**, 1195 (1993).

[38] Normally, resonance conditions on the involved frequencies determine the particular pumping (carrier or sideband) through the RWA.

[39] These dressed states differ from the ones defined in Sec. II B.

[40] V. Man'ko, G. Marmo, A. Porzio, S. Solimeno, and F. Zaccaria, Phys. Rev. A **62**, 053407 (2000).

[41] W. Vogel and R. L. de Matos Filho, Phys. Rev. A **52**, 4214 (1995).

[42] R. W. Robinett, Phys. Rep. **392**, 1 (2004).

[43] C. S. Jia, J. Y. Wang, S. He, and L. T. A. Sun, J. Phys. A **33**, 6993 (2000); A. N. F. Aleixo, A. B. Balantekin, and M. A. C. Ribeiro, *ibid.* **33**, 3173 (2000); S. Wallentowitz, I. A. Walmsley, L. J. Waxer, and Th. Richter, J. Phys. B **35**, 1967 (2002);

A. N. F. Aleixo and A. B. Balantekin, J. Phys. A **38**, 8603 (2005); J. J. Pena, M. A. Romero-Romo, J. Morales, and J. L. Lopez-Bonilla, Int. J. Quantum Chem. **105**, 731 (2005); S. H. Dong, *Factorization Methods in Quantum Mechanics* (Springer, Berlin, 2007).

[44] L. D. Landau, Phys. Z. Sowjetunion **2**, 46 (1932); C. Zener, Proc. R. Soc. London, Ser. A **137**, 696 (1932).

[45] A. S. Davydov, *Quantum Mechanics*, 2nd ed. (Pergamon, Oxford, 1976).

[46] I. Cusumano, A. Vaglica, and G. Vetri, Phys. Rev. A **66**, 043408 (2002); J. Larson, J. Salo, and S. Stenholm, *ibid.* **72**, 013814 (2005).

[47] P. F. Góra and C. Jedrzejek, Phys. Rev. A **48**, 3291 (1993); **49**, 3046 (1994); I. Sh. Averbukh, Phys. Rev. A **46**, R2205 (1992)

[48] H. Tal-Ezer and R. Kosloff, J. Chem. Phys. **81**, 3967 (1984).

[49] H. Araki and E. Lieb, Commun. Math. Phys. **18**, 160 (1970).

[50] J. H. Eberly, N. B. Narozhny, and J. J. Sanchez-Mondragon, Phys. Rev. Lett. **44**, 1323 (1980); G. Rempe, H. Walther, and N. Klein, *ibid.* **58**, 353 (1987); M. Venkata Satyanarayana, P. Rice, R. Vyas, and H. J. Carmichael, J. Opt. Soc. Am. B **6**, 228 (1989); M. Fleischhauer and W. P. Schleich, Phys. Rev. A **47**, 4258 (1993).

[51] These states are not necessarily squeezed into the proper definition, but their phase-space distributions are elliptic rather than circular.

[52] N. V. Vitanov, Phys. Rev. A **59**, 988 (1999).

[53] B. M. Garraway and S. Stenholm, Phys. Rev. A **45**, 364 (1992); B. M. Garraway and N. V. Vitanov, *ibid.* **55**, 4418 (1997); J. Larson, *ibid.* **73**, 013823 (2006).

[54] The way we define the Wigner distribution for multilevel systems by tracing out the ionic internal degrees of freedom (27) naturally destroys any information contained in the coherent crossing terms.

[55] E. Romera and F. de los Santos, Phys. Rev. Lett. **99**, 263601 (2007).

[56] R. G. Brewer, R. G. DeVoe, and R. Kallenbach, Phys. Rev. A **46**, R6781 (1992); J. Walz, I. Siemers, M. Schubert, W. Neuhauser, and R. Blatt, Europhys. Lett. **21**, 183 (1993).